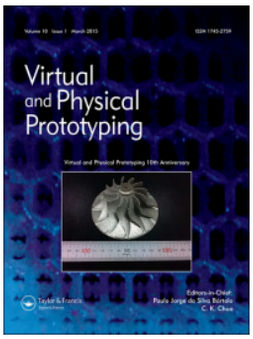

Virtual and Physical Prototyping

ISSN: 1745-2759 (Print) 1745-2767 (Online) Journal homepage: www.tandfonline.com/journals/nvpp20

Integrated numerical modelling and deep learning for multi-layer cube deposition planning in laser aided additive manufacturing

K. Ren, Y. Chew, N. Liu, Y. F. Zhang, J. Y. H. Fuh & G. J. Bi

To cite this article: K. Ren, Y. Chew, N. Liu, Y. F. Zhang, J. Y. H. Fuh & G. J. Bi (2021) Integrated numerical modelling and deep learning for multi-layer cube deposition planning in laser aided additive manufacturing, Virtual and Physical Prototyping, 16:3, 318-332, DOI: 10.1080/17452759.2021.1922714

To link to this article: https://doi.org/10.1080/17452759.2021.1922714

VIRTUAL AND PHYSICAL PROTOTYPING
2021, VOL. 16, NO. 3, 318–332
https://doi.org/10.1080/17452759.2021.1922714

Taylor & Francis
Taylor & Francis Group

Integrated numerical modelling and deep learning for multi-layer cube deposition planning in laser aided additive manufacturing

K. Ren [a], Y. Chew[a], N. Liu [b], Y. F. Zhang[c], J. Y. H. Fuh [c] and G. J. Bi[a]

[a]Singapore Institute of Manufacturing Technology, Agency for Science, Technology and Research, Singapore; [b]Advanced Remanufacturing and Technology Centre, Agency for Science, Technology and Research, Singapore; [c]Department of Mechanical Engineering, National University of Singapore, Singapore

ABSTRACT

Heat accumulation is a critical problem in continuous multi-layer laser aided additive manufacturing (LAAM) process, resulting in inhomogeneous mechanical properties and non-uniformity in the deposited height which can deteriorate the deposition process. This work presents a new integrated finite element (FE) simulation and machine learning approach to select a multi-layer laser infill toolpath planning strategy for fabricating quadrilateral parts to minimise localised heat accumulation during the deposition process. After one layer deposition simulation, the approach employs a Temperature-Pattern Recurrent Neural Networks (TP-RNN) model to predict the temperature field after the next layer deposition for each of the candidate infill toolpaths, and a process parameters inspired thermal field evaluation method to select the best candidate toolpath. The approach would significantly improve the computational efficiency of the laser infill toolpath planning, which was validated by improving the flatness of the 20-layer cube deposition samples with two dimensions (20 mm × 20 mm and 30 mm × 30 mm).

ARTICLE HISTORY
Received 7 March 2021
Accepted 23 April 2021

KEYWORDS
Laser aided additive manufacturing; multi-layer deposition; thermal analyses; recurrent neural networks; toolpath planning

1. Introduction

Laser Aided Additive Manufacturing (LAAM), categorised under Directed Energy Deposition (DED), is a metal additive manufacturing (AM) technology known for high deposition rate and suitable for large format 3D deposition processes (Herzog et al. 2016). It utilises a high power laser beam to melt the additive material in the powder or wire form delivered into the melt-pool for cladding or fabricating a near-net-shape part (Mazumder 2016). Apart from applications such as surface modification (Fesharaki et al. 2018) and repairing defective components (Zhang, Li, et al. 2018), the material incremental build-up philosophy and a multi-axis computer numerical control (CNC) machine or robot utilised in LAAM make it possible to build complex parts. Compared with the conventional subtractive manufacturing, AM improves the deposition efficiency, expands the design possibilities, and reduces the material wastage (Gu et al. 2012). However, deposition using a high power laser (DebRoy et al. 2017) will tend to input heat energy at the surface more rapidly than heat dissipation into the substrate and to the ambient. In the multi-layer deposition, the accumulated heat within the existing part reduces the solidification rate and changes the deposited bead profile and the local build height. In the case of the blown powder process, if the height deviation is within the depth of the powder focus, the deposition process can self-regulate itself to a stable status (Haley et al. 2019). Otherwise, the height deviation will be accumulated over subsequent layers until the deposition process is unstable using the pre-programmed process parameters, causing disruptions to the deposition processes and can even damage the powder feeding nozzle. The surface oxidation also needs to be avoided to maintain the stability of the melt-pool and the deposition process (Bi, Sun, and Gasser 2013).

Improving the homogeneity of the temperature distribution is useful to maintain the stability of the deposition process. Laser toolpath planning is one key important strategy to mitigate heat accumulation in the multi-layer LAAM deposition process. Moreover, the selected infill strategy can be reused for the new deposition process (of the same part) and transferrable for other parts with similar geometries without having to perform the finite element (FE) simulation again.

Existing works on laser deposition toolpath planning can be categorised into two general approaches. The first type is 'geometry-inspired', which focuses on designing an integrated toolpath from single-layer deposition to entire component deposition sequence. It aims to avoid voids generated due to the incomplete

CONTACT Y. Chew chewyx@simtech.a-star.edu.sg; G. J. Bi gjbi@SIMTech.a-star.edu.sg
This article has been republished with minor changes. These changes do not impact the academic content of the article.

infill from the toolpath planning (Ren et al. 2010). Different approaches like the single continuous toolpath strategy (Venturini et al. 2018), multi-direction slicing algorithms (Ding et al. 2016) and medial axis method (Ding et al. 2016), were developed to optimise the deposition toolpaths. The second type is 'property-inspired' that aims to optimise the toolpath to improve the mechanical properties, e.g. stress concentration, distortion, flatness. Early research investigates the influence of the basic spiral or zigzag scanning strategies on the distortion (Dai and Shaw 2002), followed by further research on using the fractal deposition pattern (Yu et al. 2011) or the island scanning pattern to reduce part distortion (Foroozmehr and Kovacevic 2010). Toolpath with shorter dwell time between adjacent layers would reduce the residual stress and distortion (Denlinger et al. 2015). The significant deviation of the defined increment in Z-direction from the actual layer thickness can cause unstable melt-pool and deterioration of the LAAM process (Bi et al. 2006). Appropriate process parameters can be acquired by the experiments and mathematical analysis (Campanelli et al. 2017; Angelastro, Campanelli, and Casalino 2017). These works rely on empirical experiments and analysis. Comparatively, finite element (FE) analysis uses a numerical evaluation method in toolpath planning. Early exploration focussed on improving the simulation accuracy by using quiet or inactive element methods to describe material increasing (Michaleris 2014), or fully-coupled thermo-mechanical analysis to predict thermal related stress behaviour (Lindgren et al. 2016; Tan, Sing, and Yeong 2020). The capability of FE model simulation has also improved with better computing power from single track simulation to entire part simulation (Nie et al. 2016; Song et al. 2018), while the simulation time for a single deposition case can range from several hours to several days depending on the scale, geometrical complexity and mesh selection. The FE modelling thus has demonstrated capabilities to increase the toolpath planning efficiency by replacing the empirical trials and errors with numerical simulations, and improve the toolpath planning accuracy by simulating the complex physical phenomenon during the deposition. However, the computation cost remains an obstacle for the effective toolpath planning.

The emerging deep learning technologies (LeCun, Bengio, and Hinton 2015) demonstrate significant potential to improve the toolpath planning efficiency in LAAM. The calibrated FE model can generate sufficient data without measurement noise to construct the training dataset, which is critical in training deep learning models. Our previous work has designed a machine learning model to predict the output temperature field by a given laser scanning status (Ren et al. 2019). The work presented in this paper further utilises an integrated numerical modelling and machine learning approach to address the multi-layer cube deposition toolpath planning problem. Specifically, the contributions of the presented work include: (i) designing a TP-RNN model to predict the temperature field of the next depositing layer using the inputs from the simulated thermal field of the previous two deposited layers and the candidate toolpaths; (ii) designing an integrated FE model and machine learning model approach to iteratively evaluate and select toolpaths layer by layer during the simulation; (iii) designing a process parameter inspired heat accumulation metric to evaluate the laser infill toolpath strategies. The work would significantly improve the toolpath planning efficiency from the conventional FE modelling approach. The selected toolpath would minimise localised heat accumulation during the deposition, further improving the homogeneity of the temperature distribution by adjusting infill strategy used in each layer during the entire deposition process.

2. Methodology

2.1. Toolpath planning for multi-layer deposition

Toolpath planning for multi-layer deposition of cubes involves selecting appropriate deposition toolpath for the entire part, which can be gradually resolved by going through the following (i) selecting a infill toolpath for each layer, (ii) selecting a starting point for each selected infill toolpath and (iii) combining infill toolpath for each layer to construct the infill toolpath for the entire component. In this study, the following assumptions are preset to define the research problem:

(1) The deposition parts are cubes, while edge length of the cube l_{edge} is the parameter that can be modified for different parts.
(2) Zigzag patterns (x- and y-directional) are selected as the basic infill toolpath as they are widely applied in the LAAM process. Four corner points (A, B, C and D, anti-clockwise starting from the left bottom corner) were selected as starting points. As such, a set of eight possible infill toolpath, P_{set} (XA, XB, XC, XD, YA, YB, YC and YD, respectively), was formed, as illustrated in Figure 1. The prefix, 'X' and 'Y' refers to the zigzag scanning direction used in tandem with the starting positions A, B, C or D. In addition, for the XA scanning pattern, if the laser scanning track number is odd, the laser ends at the top right corner, whereas if the laser scanning track number is even, the laser ends at the top left corner.

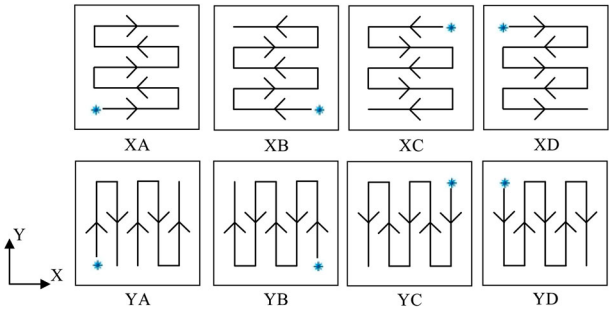

Figure 1. Infill toolpath set, XA represents along x-direction and starting at point A (* indicates the infill starting corner point).

(3) The scanning direction was designed to be perpendicular in adjacent layers to improve the flatness of the deposited component. Therefore, in odd layers, the infill direction was set along the *x*-direction, whereas the y-direction was chosen for even layers.

In this study, the zigzag infill toolpaths (along the *x*- and *y*-directions) were selected as the basic infill toolpath. The unidirectional toolpaths (offset pattern) are not considered due to longer deposition time required for the robot or CNC to return to the side of the starting line, before depositing the subsequent tracks. It is also not commonly used as it affects the uniformity of the deposited material, since the built height varies along the deposited track in LAAM processes. Thus, a bias in the deposition direction is generally observed. Spiral toolpath is also not commonly used for building regular geometry such as a cube. In a spiral toolpath, such as the spiral-inwards toolpath, the scan-length of the depositing tracks will vary spatially and gets shorter towards the centre. Thus, it is expected that the heat accumulation near the centre will be higher, due to shorter time cooling interval between overlapping laser passes. These analyses show the spiral toolpath is also not a generic or characteristic toolpath used in LAAM processes.

The possible infill toolpaths for cube deposition can then be derived via enumeration. With one infill toolpath selected for a given layer, four candidate infill toolpaths are available for the next layer. Hence, for an *n*-layer cube deposition, the toolpath planning is to select the best toolpath strategy from the 4^{n-1} possible combinations of the infill toolpaths, as shown in Figure 2.

It was evident that the number of the possible toolpaths for building the cube grows exponentially with the increase of the number of the deposited layers. The large quantity of the infill toolpaths makes it virtually impossible to simulate every possible case and select an appropriate and optimal case with existing computational capabilities. Therefore, in this paper, we propose an iterative toolpath planning approach to evaluate and choose the infill toolpath layer by layer. After simulating the one-layer deposition, the approach will predict the temperature field of the next-to-be-deposited layer for each of the four possible infill toolpaths using a developed machine learning model. The infill toolpath providing the most homogeneous temperature distribution is chosen and used for depositing the next layer, as illustrated in Figure 3. For the infill toolpath planning of an *n*-layer cube, the proposed approach can significantly reduce the simulation cases from 4^{n-1} to 1.

In the proposed toolpath planning approach, a TP-RNN model is trained to predict the temperature field outcome of one layer based on the temperature field of the previous two layers and the selected infill toolpath. The details of the TP-RNN model will be introduced in Section 2.2 and the architecture of the infill toolpath planning approach is introduced in Section 2.3.

2.2. TP-RNN model

The TP-RNN model is introduced in this section to further elaborate on the thermal history dataset preparation, TP-RNN data structure design and TP-RNN algorithm design.

2.2.1. Thermal history dataset preparation

The experimental calibrated LAAM thermal analyses FE model developed in our previous work was used in the dataset construction (Ren et al. 2019). The simulation of depositing a cube with the edge length l_{edge} equalling 11 mm was designed for the dataset building. The cube was designed to be deposited at the centre of a 50 mm × 50 mm × 5 mm substrate, as illustrated in Figure 4. Eight infill toolpaths as described in Section 2.1 were used to build the cube. Therefore, a total of 340 $(4^4 + 4^3 + 4^2 + 4^1)$ infill toolpath combinations for five layers were simulated to form the dataset.

The geometry of the unit domain in the simulation was calibrated as $1.1 \times 1.1 \times 0.5\ mm^3$, where a 50% overlap rate was utilised during the deposition. Other process parameters are listed in Table 1. Two workstations (104 GB RAM and a 6-core 3.20 GHz CPU, 32 GB RAM and a 10-core 2.20 GHz CPU) were used and it took approximately three months to collect all the thermal history data required for constructing the dataset.

2.2.2. Data structure design

The thermal history data stored in the dataset were used to train the neural networks model describing the

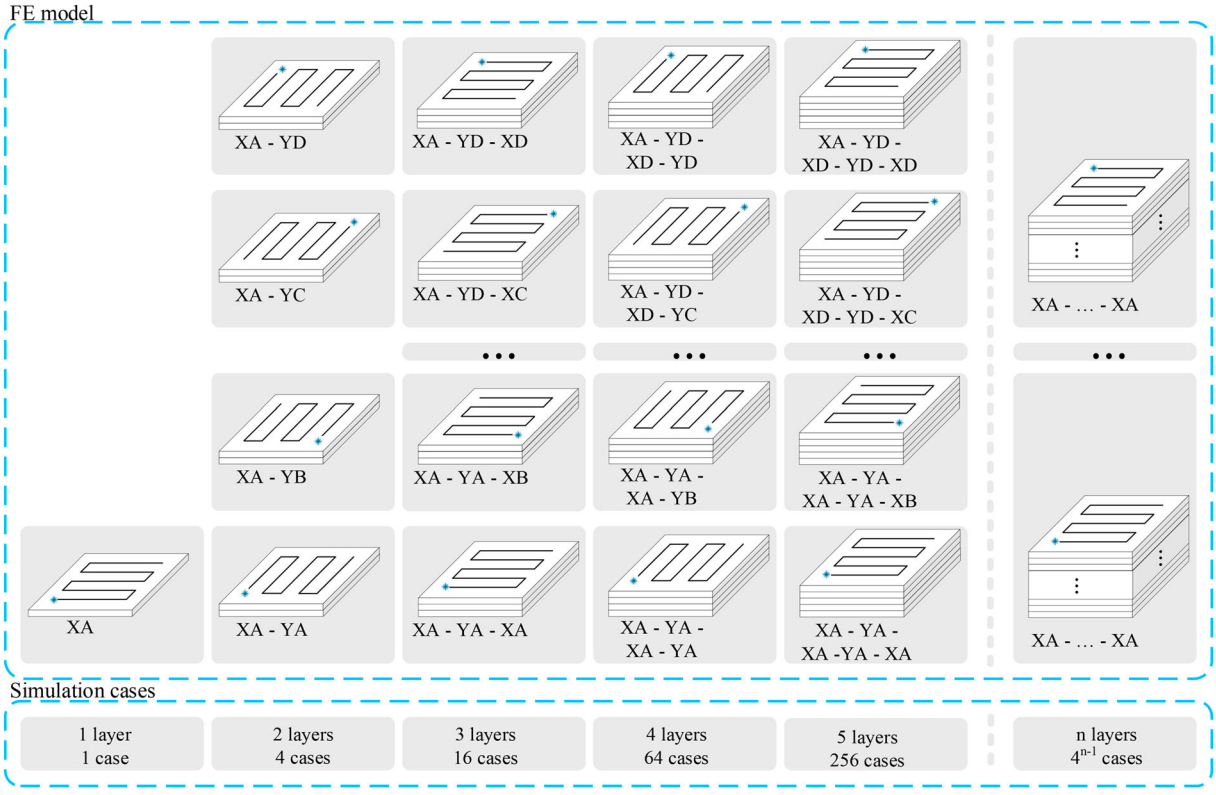

Figure 2. Conventional FE model toolpath planning approach (XA – YA – XA – YA – XA indicates the XA, YA, XA, YA and XA are selected as infill toolpath for the first to the fifth layer, respectively).

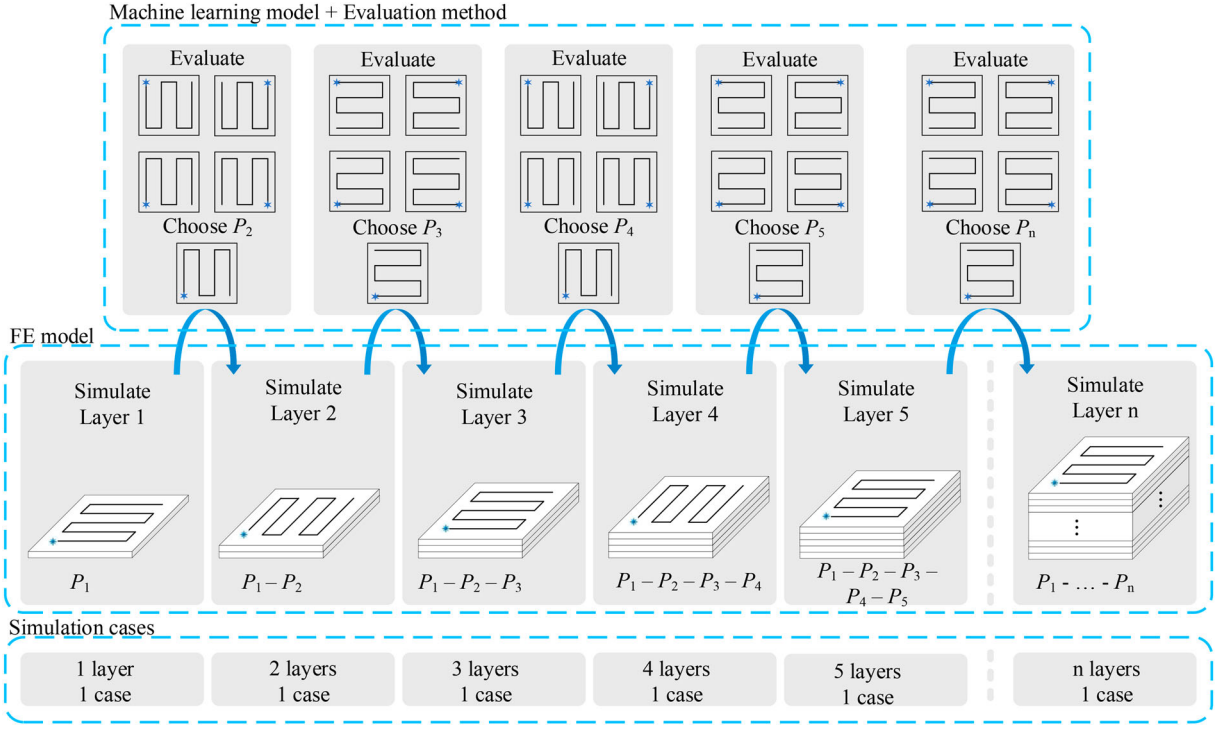

Figure 3. Proposed toolpath planning approach (P_n indicates the infill toolpath selected for nth layer, chosen from the infill toolpath set).

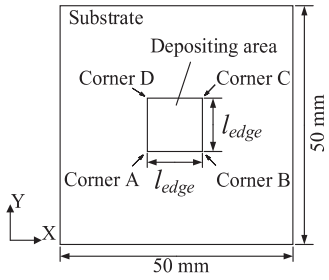

Figure 4. Schematic drawing of the cube and substrate for preparation of the thermal history dataset.

relations among the temperature fields of different layers and the infill toolpaths used. A uniform 10×10 data matrix T^i_{tem} was designed to describe the temperature field of layer L_i, which helps to maintain consistency in data structure when describing cubes with different l_{edge}. The element $t_{m,n}$ (m, n ε [1,10]) in the matrix T^i_{tem} represents the mean temperature of the block $b_{m,n}$ of the layer L_i. For cubes with different sizes, the dimensions of the block $b_{m,n}$ will change accordingly to maintain the 10×10 blocks discretisation of one layer. In the thermal history dataset preparation described in section 2.2.1, the dimension of one deposition layer is $11 \times 11 \times 0.5$ mm^3. Therefore the dimension of the unit block $b_{m,n}$ is $1.1 \times 1.1 \times 0.5$ mm^3. The temperature inspection node was defined at the corner point of a unit sampling cell in the FE model. The dimension of the sampling unit in this study is $0.1 \times 0.1 \times 0.5$ mm^3. In the thermal history dataset, the original dimension of the temperature inspection node matrix is $110 \times 110 \times 2$ (with top and bottom surface having 110×110 points respectively). The temperature feature extraction method is illustrated in Figure 5.

The infill toolpaths listed in Section 2.1 were described using temperature field T^1_{tem} derived from corresponding infill toolpath, i.e. $T_{\text{pat}=\text{XA}}$ is defined by $T^1_{\text{tem, pat}=\text{XA}}$. Therefore, single-layered cube deposited with toolpaths from P_{set} was simulated additionally to form the T_{pat}, as illustrated in Figure 6. Choosing a temperature-based dataset to express the infill toolpath has improved consistency for integrating the predicted thermal field data from different layers, enabling the model to establish a correlation of the thermal fields among different layers.

Table 1. Process parameters of the LAAM.

Laser related parameters	Laser beam radius r	1×10^{-3} m
	Initial laser power P	1.07×10^3 W
	Laser scanning speed v	2×10^{-2} m/s
	Laser absorptivity	0.42
Material related parameters	Material properties	Stainless steel 316L
	Powder flow rate	16.6 g/min
	Powder absorption rate	50%
	Powder initial temperature	1723K
	Overlap ratio	50%
Substrate related parameters	Substrate initial temperature	293 K

2.2.3 Structure of the TP-RNN model

In multi-layer LAAM process, the temperature field is influenced by different process parameters, including laser power, laser scanning speed, overlap ratio, powder type, powder feed rate and infill toolpath, etc. When the process parameters except the infill toolpath are kept constant, the temperature field of the next depositing layer (after deposition) can be derived from the temperature field of the current depositing layer, previously deposited layers and the infill toopath of the next depositing layer, described as $f(T^{i-1}_{\text{tem}}, T^i_{\text{tem}}, T^{i+1}_{\text{pat}}) \rightarrow T^{i+1}_{\text{tem}}$.

The machine learning model utilises an RNN hidden layer (500 long short memory cells, LSTM) and a fully connected layer (200 neurons) to represent the function f, as illustrated in Figure 7. The RNN model with LSTM structures was selected as it performs better than the Deep Neural Networks (DNN) and the Convolutional Neural Networks (CNN) structure in the preliminary trial and error studies, which demonstrated good capabilities in describing the temporal and spatial relations in numerical modelling of LAAM process (Ren et al. 2020).

During the training process, the rectified linear unit (ReLU) was selected as the activation function. The normalised mean square error (nMSE) was chosen as the evaluation matric, as defined in Equation (1), where $\widehat{y_i}$ represents the TP-RNN model predicted temperature field, and y_i is the ground truth temperature field in the dataset. The parameters in the TP-RNN model were optimised using the Adaptive Moment Estimation (Adam) method (Ruder 2016).

$$\text{nMSE} = \frac{1}{n}\sum_{i}^{n}(y_i - \hat{y}_i)^2 \tag{1}$$

2.3. Process parameter inspired thermal field evaluation method

A heuristic process parameter inspired thermal field evaluation method was developed to evaluate the heat accumulation situation during the multi-layer deposition process. The method is based on the following considerations: (i) The heat accumulation situation in multi-layer deposition is related to the increase in the temperature of the newly deposited layers and the volume of the melt-pool; (ii) Compared with the temperature increase outside of the melt-pool, the

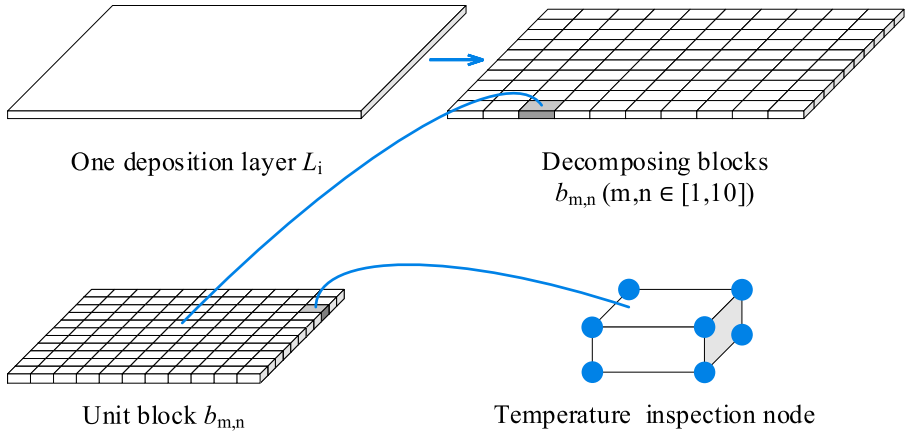

Figure 5. Generation of uniform temperature field graph.

temperature increase within the melt-pool (especially the area within the laser beam radius r) is relatively small; (iii) as the deposition layer increases, the effect of the newly deposited layer on the heat accumulation decreases as the deposited part has gradually contained more heat in the part.

A weighted temperature matrix T_w^i was designed to describe the heat accumulation situation after the deposition of layer L_i. The element $t_{w;l,m,n} \varepsilon T_w$ ($l \varepsilon [1, 2, 3, \ldots, i+1]$; $m, n \varepsilon [1,10]$) is defined in Equation (2), where $w_{l,m,n}$ is the weight coefficient assigned on the block $b_{m,n}$ of the layer L_i, and $t_{m,n}$ is the mean temperature of the same block $b_{m,n}$ calculated according to the elaboration in sections 2.2.2 and 2.2.3. The weight calculation function was designed based on the Gaussian distribution. The mean μ and the variance σ^2 were selected with relation to the laser beam radius r (in this work, $\mu = 12r$ and $\sigma^2 = 6r$), and parameter α indicates the influence of the existing part and the next layer (in this work, $\alpha = 10$ for $l \leq i$ and $\alpha = 1$ for $l = i+1$). The distance between the centre point of the block $b_{m,n}$ (x_b, y_b, z_b) and the reference point P_0 (x_0, y_0, z_0) in each candidate patterns is used to calculate the weight $w_{l,m,n}$. For a given candidate pattern, P_0 was selected as the laser start point when $l \leq i$ and the laser end point when $l = i+1$, with one example coefficient matrix $w_{l=i+1,m,n}$ illustrated in Figure 8.

$$t_{w;l,m,n} = w_{l,m,n} \times t_{m,n}\ ,\ (t_{m,n} \in T_{\text{tem}}^{l})$$
$$\text{where } w_{l,m,n} = \frac{\alpha}{\sigma\sqrt{2\pi}} e^{-0.5((\text{dist}-\mu)/\sigma)^2} t_{m,n}\ ,\ (t_{m,n} \in T_{\text{tem}}^{l})$$
$$\text{dis} = \sqrt{(x_b - x_0)^2 + (y_b - y_0)^2 + (z_b - z_0)^2} \tag{2}$$

A heat accumulation metric H was further designed based on the weighted temperature matrix T_w, as defined in Equation (3). A smaller H would indicate

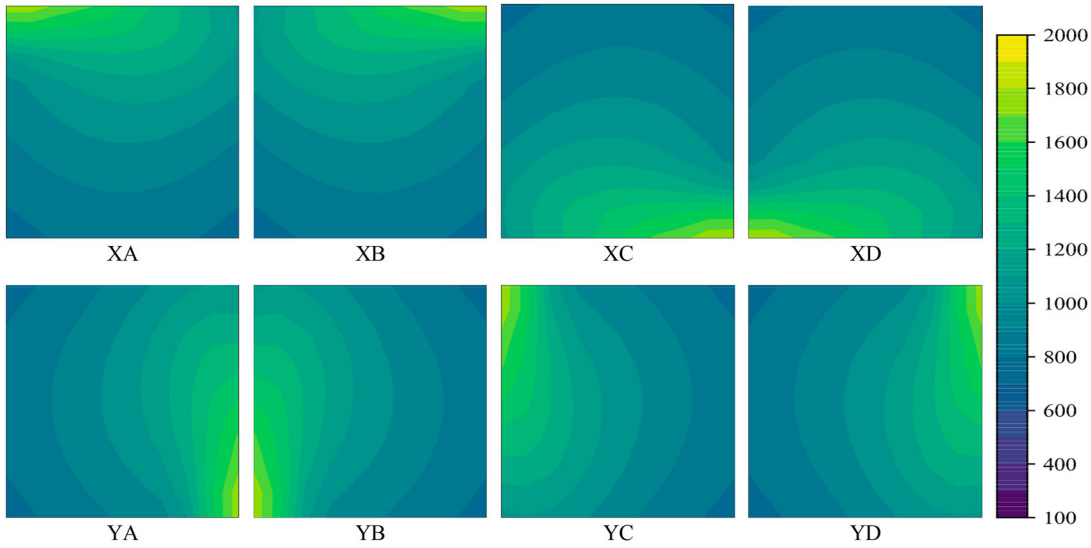

Figure 6. Temperature contour graph of the T_{pat} (even tracks) for a single layer (unit: °C).

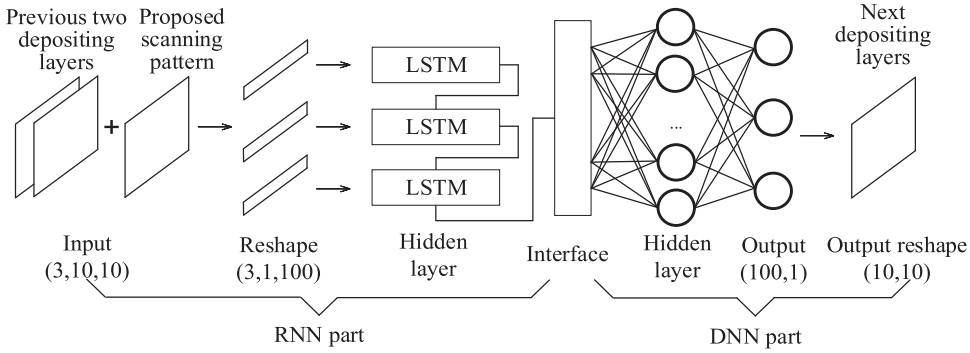

Figure 7. Structure of the RNN-DNN model.

lesser extent of localised heat accumulation during the deposition process. It should be highlighted that the parameter selected in these metrics are based on the heat accumulation investigation stated in previous paragraphs and can be further improved in future work.

$$H= \begin{cases} \frac{1}{i+1}\left(\sum_{l=1}^{l=i}\sum_{m=1,n=1}^{m=10,n=10} t_{w;l,m,n}+\frac{1}{2i}\sum_{m=1,n=1}^{m=10,n=10} t_{w;i+1,m,n}\right), L_i \le L_3 \\ \frac{1}{4}\left(\sum_{l=i-3}^{l=i}\sum_{m=1,n=1}^{m=10,n=10} t_{w;l,m,n}+\frac{1}{2i}\sum_{m=1,n=1}^{m=10,n=10} t_{w;i+1,m,n}\right), L_i > L_3 \end{cases} \quad (3)$$

2.4. Infill toolpath planning approach for multi-layer LAAM

The proposed infill toolpath planning approach consists of the FE model, the TP-RNN model and the evaluation method, as illustrated in Figure 9. At the beginning, the laser beam and material related process parameters are imported to define the boundary condition and initial condition. The infill toolpath for the first depositing layer is predefined to guide the simulation domain adding sequence. Once the deposition simulation of a layer is completed, the temperature field for the next depositing layer is predicted via the TP-RNN model. The predicted temperature field matrix T_{tem}^{i+1} output is integrated with the existing temperature field matrixes T_{tem}^{j} ($j = 1, 2, 3, \ldots, i$) to describe the temperature field of the entire part after the end of the deposition for the next layer. The heat accumulation metric H is calculated to describe the heat accumulation simulation for each candidate infill toolpaths. The infill toolpath that generates the minimum H is selected for the next layer. When the entire deposition simulation is completed, the selected infill toolpath sequence for each layer are exported as the optimised toolpath for the deposited cube. The LAAM multi-layer infill toolpath planning approach was built using commercialised software MATLAB, COMSOL and open-source Python and Pytorch.

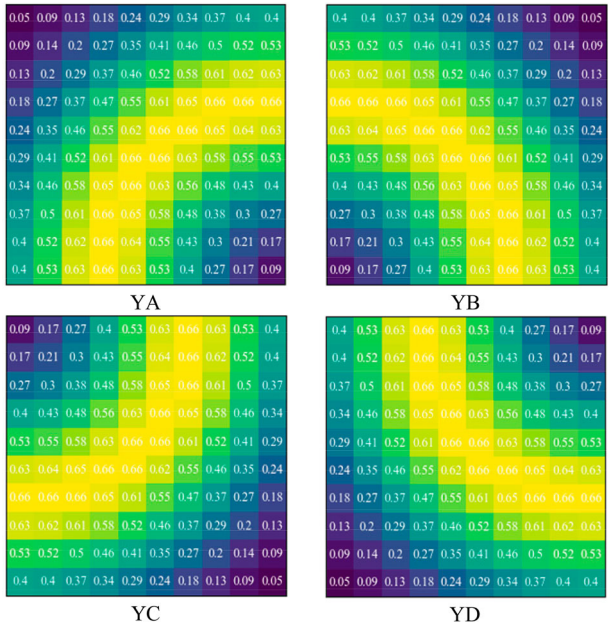

Figure 8. Illustration of weight function $w_{l,m,n}$ ($l = i+1 = 2$; unit: 1).

Heat accumulation situation is selected as the evaluation criterion in the infill toolpath planning approach. Apart from delaying the onset of process instability, the heat accumulation situation could also affect the temperature distribution homogeneity, which further influence the overall part distortion (Yan et al. 2018). In this work, the TP-RNN model describes the connection between the temperature field of two previously deposited layers, selected infill toolpath, and the temperature field for the next deposition layer. Thus, the LAAM multi-layer infill toolpath planning approach is applicable for planning infill toolpath beyond the number of simulated layers in the thermal history dataset. Nevertheless, dataset with more layers and infill toolpath combinations can improve the predication accuracy of the TP-RNN model, which will be included in the future work with availability of improved computational capability.

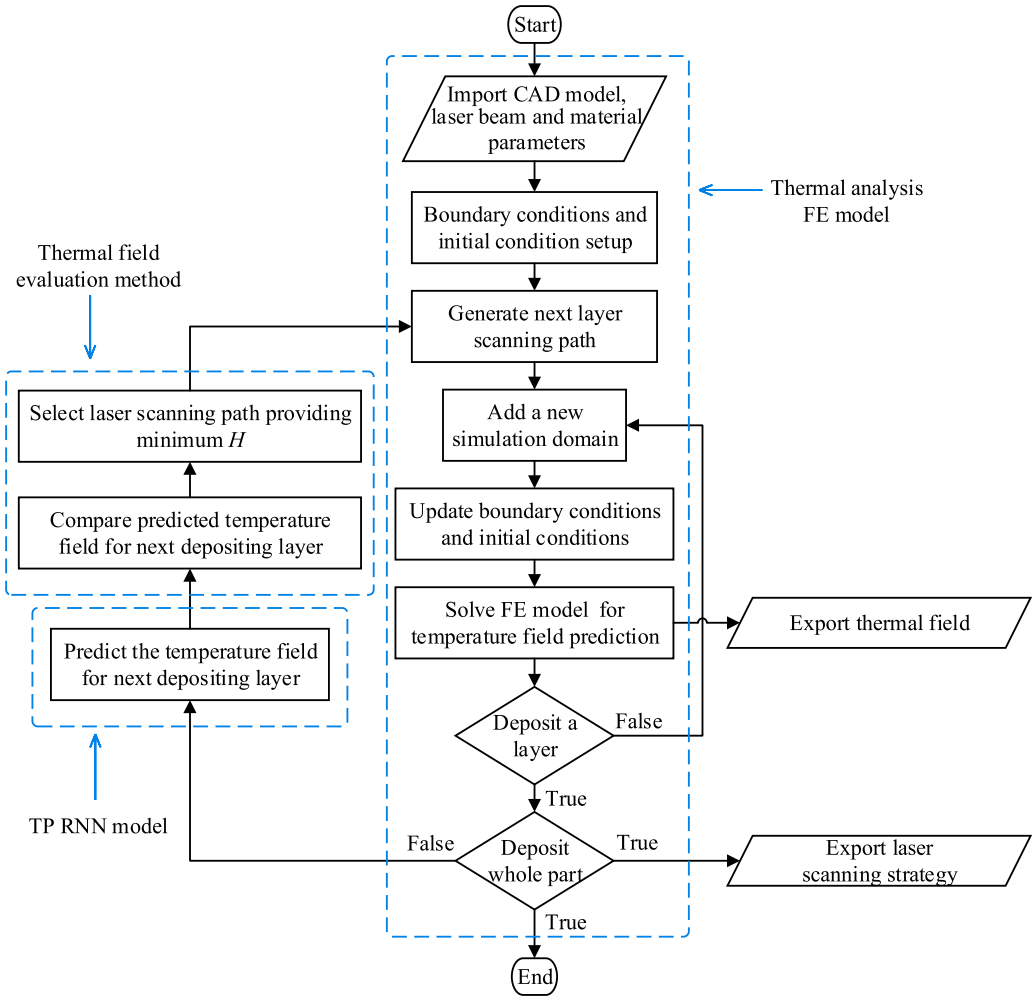

Figure 9. Flow chart of the infill toolpath planning approach for multi-layer LAAM.

3. Experiment and results

3.1. Training of the inter-layer temperature field prediction algorithm

The thermal history dataset described in Section 2.2.1 includes 340 inter-layer temperature field prediction cases (accumulated from simulation database from $L_1 \rightarrow L_2$, $L_2 \rightarrow L_3$, $L_3 \rightarrow L_4$ and $L_4 \rightarrow L_5$ respectively). In the data pre-processing phase, the data was split into the training set and test set with the ratio of 9:1. The batch size was set as 1. The nMSE on the training test and accuracy on the test sets were recorded for every epoch, whereby the expression used to determine accuracy is given in Equation (4). The computations were performed on windows 64-bit PC, including a 64 GB RAM, an 8-core 3.80 GHz CPU and a NVIDIA GeForce GTX 2080 Ti GPU. All training and validation are implemented with Pytorch.

$$\text{Accuracy} = \frac{1}{n}\sum_{i=1}^{n}\frac{y_i - \hat{y}_i}{y_i} \times 100\% \quad (4)$$

The training process is shown in Figure 10, where the training loss and test accuracy are recorded along with training epochs. It can be observed that the loss curve for the TP-RNN model decreases from over 100,000 and converged to below 20,000 after 500 epochs. Meanwhile, the accuracy curve increased quickly and achieved over 90% after 100 epochs. The accuracy of the model trained for 1000 epochs is 95.05%, implying the TP-RNN model fits the function f well.

3.2. Validation of the infill toolpath planning through simulation

To validate the proposed multi-layer infill toolpath planning approach, a 10-layer stainless steel 316L cube was designed to be deposited at the centre of the substrate illustrated in Figure 4, with the edge length l_{edge} equals 20 mm. The results of the infill toolpath planning using the infill toolpath planning approach are summarised in Table 2, with P_1 defined as XA. Each row records the heat accumulation metric H values calculated by the different

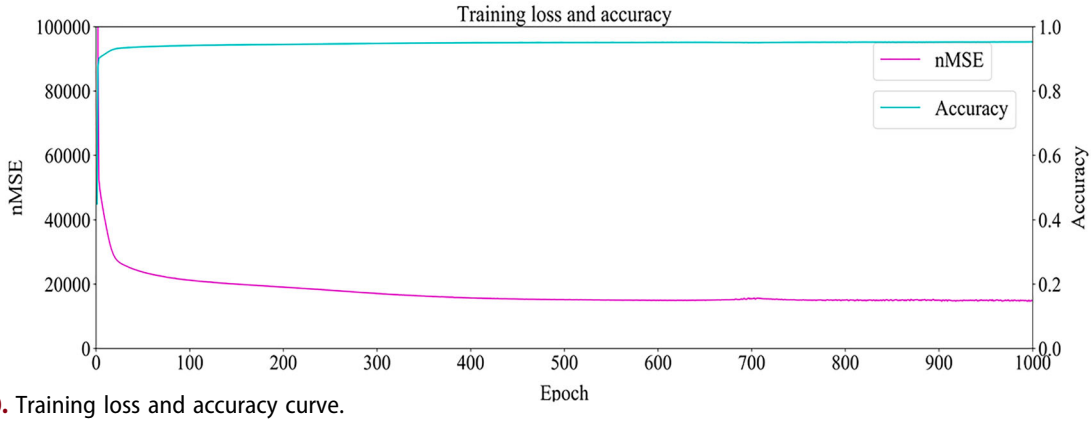

Figure 10. Training loss and accuracy curve.

candidate infill toolpaths for the next layer L_{i+1}. The corresponding infill toolpath with the lowest H values is marked with an '*' and selected as the recommended optimal P_{i+1} toolpath. The prefix, 'X' and 'Y' in the last column refers to the zigzag scanning direction used with the starting positions A, B, C or D. The integrated approach predicts that the optimised starting point selection for the depositing multi-layer cube follows the sequence of A-B-C-D, which repeats after every four layers. It indicated that the anti-clockwise infill toolpath sequence provides better cooling conditions for the deposition of the subsequent new layer when building a cube based on the current evaluation criteria.

3.3. Validation of infill toolpath planning through experiments

The anti-clockwise infill toolpath strategy observed in section 3.2 was further evaluated and verified using different deposited cubes dimensions. Two different sizes (l_{edge} equals 20 mm and 30 mm) of 20 layers cubes were deposited in the experiment setup illustrated in Figure 4, via four different infill toolpaths strategies (anti-clockwise: XA-YB-XC-YD, diagonal: XA-YC-XA-YC, switch: XA-YB-XA-YB and random: (XA or XB or XC or XD)-(YA or YB or YC or YD)). The same starting point deposition infill toolpath (XA-YA-XA-YA) was not utilised as it intuitively leads to inhomogeneous thermal distribution and may not provide a good comparison to the selected toolpath. The deposited cubes were scanned by 3D scanner Solutionix C500 with FOC175 with the accuracy of ±10 μm tolerance, as illustrated in Figure 11.

Table 2. Summary of infill toolpath planning.

Layer L_i (simulation)	Heat accumulation metric H				Toolpath P_{i+1} (planning)
	Start at A	Start at B	Start at C	Start at D	
L_1	307.73	**301.86**[a]	311.82	324.02	P_2 = YB
L_2	258.47	258.52	**255.19**[a]	266.91	P_3 = XC
L_3	273.09	269.48	258.89	**258.40**[a]	P_4 = YD
L_4	**269.38**[a]	287.97	285.96	272.24	P_5 = XA
L_5	267.87	**266.03**[a]	281.07	280.43	P_6 = YB
L_6	291.27	281.17	**279.39**[a]	294.73	P_7 = XC
L_7	304.69	301.64	290.01	**289.05**[a]	P_8 = YD
L_8	**295.96**[a]	312.53	310.59	298.20	P_9 = XA
L_9	307.24	**305.79**[a]	321.28	320.22	P_{10} = YB
L_{10}	329.74	318.26	**316.86**[a]	332.39	P_{11} = XC

[a]Indicates the minimum value of the H.

The flatness variance of the top surface V_{fla} of the deposited sample was selected as the metric to evaluate the infill toolpath sequence. The calculated V_{fla} is illustrated in Figure 12 and via the following steps:

(1) Determine the x–y plane centre of the scanned file M. The cross-section surface at 1 mm height of the mesh M was used to find the centroid of the plane.
(2) Trim the scanned file M_{trim} to form a square (18 mm × 18 mm and 28 mm × 28 mm for two

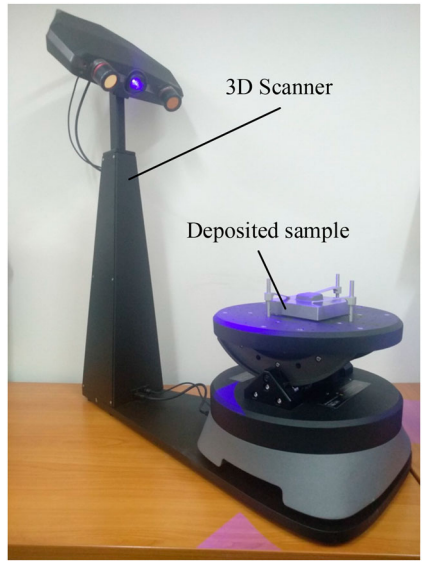

Figure 11. Deposited sample 3D scanning set up.

different cube sizes respectively, maintaining 1 mm distance to the boundary) centric with the original top surface of the cube.

(3) Calculate the z coordinate p_z of point p ($p \in M_{\text{trim}}$) with 1 mm resolution and the flatness variance V_{fla} is calculated using Equation (5), where *num_x* and *num_y* are the number of points along the x- and y-direction, respectively.

$$V_{fla} = \frac{1}{num_x \times num_y} \sum_{i=1,j=1}^{i=num_x,j=num_y} (p_{z,i,j} - \hat{p}_z)^2,$$
$$\hat{p}_z = \frac{1}{num\_x \times num\_y} \sum_{i=1,j=1}^{i=num\_x,j=num\_y} p_{z,i,j} \quad (5)$$

The flatness variance V_{fla} of the deposited cubes is listed in Table 3, together with the trimmed scanned file M_{trim} shown in Figure 13. It is observed that the V_{fla} is lower for anti-clockwise infill toolpaths compared with other three strategies in both scale cubes (20 mm × 20 mm and 30 mm × 30 mm) deposition experiments. It suggests the anti-clockwise infill toolpath sequence performs better compared with other infill toolpath strategies, which also validate the feasibility of the proposed infill toolpath planning approach.

4. Discussion

In this paper, a TP-RNN integrated infill toolpath planning approach was developed to select the infill toolpath sequence for a cube deposition. This section provides further discussions on process planning for multi-layer cube deposition and machine learning integration.

4.1. Process planning in multi-layer cube deposition

In the multi-layer cube deposition scenario, the anti-clockwise infill toolpath strategy has demonstrated better flatness compared with other strategies. The infill toolpath selection leverages on localised temperature inhomogeneity; giving opportunities and gaps to improve the temperature distribution through optimising the laser heat input sequence. With increasing built layers, the part has more time for temperature redistribution, and melt-pool size increases due to heat accumulation. These factors result in the observed diminishing influence of infill toolpath on surface flatness. Therefore, the mitigation of the localised heat accumulation enables improvement in the temperature distribution homogeneity, which contributes to the uniformity in the deposited height and aids continuity of the deposition process.

Based on experimental observation, the inclusion of profile contouring deposition toolpath around the boundary is useful to improve the flatness of the deposited surface. However, this is not considered in the current study as the main focus was to evaluate the effects of the infill toolpath. Nonetheless, it is evident that surface flatness degrades with increasing deposition layers, reducing dimensional accuracy, and requiring intervention to restore geometry for subsequent deposition. The change in thermal condition is likely one of the main influencing factors for built surface flatness. This is consistent with the observation that the flatness variance values are lower for the deposited part with a larger cross-sectional area; attributed to better heat dissipation along the z-direction into the substrate.

The proposed LAAM infill toolpath planning approach was designed for the multi-layer cube deposition. For other LAAM deposition scenarios, like rectangles with different aspect ratios, geometries with complex features like curves and sharp turnings, the designed approach can be further improved by adjusting the TP-RNN model and the process parameters of the thermal field evaluation metric. Another observation is that the diminishing influence of the infill toolpath planning method on the heat accumulation with increasing deposition layers. This is caused by increasing heat accumulation that cannot be sufficiently mitigated by infill path selection. Hence, other methods such as variation in laser power are needed to improve the heat distribution. A combination of the infill toolpath and optimised laser power input will be studied for subsequent work to improve the consistency in thermal conditions for depositing multiple layers.

4.2. Machine learning integration

Machine learning algorithms demonstrate impressive capabilities to establish a correlation between 'feature – label' (input–output) (LeCun, Bengio, and Hinton 2015). This advanced function is also utilised to analyse additive manufacturing related data (Qi et al. 2019; Ng et al. 2020). For instance, in empirical data analysis of process parameters (Caiazzo and Caggiano 2018), deposition surface geometry (Chen et al. 2020) and image processing of melt-pool monitoring in selective laser melting (SLM) (Zhang et al. 2018). Other applications include evaluating the surface finishing quality of the extrusion-based 3D concrete printing (Lao et al. 2020), cell and cellular process parameters in bioprinting (An, Chua, and Mironov 2021), thickness of conductive lines

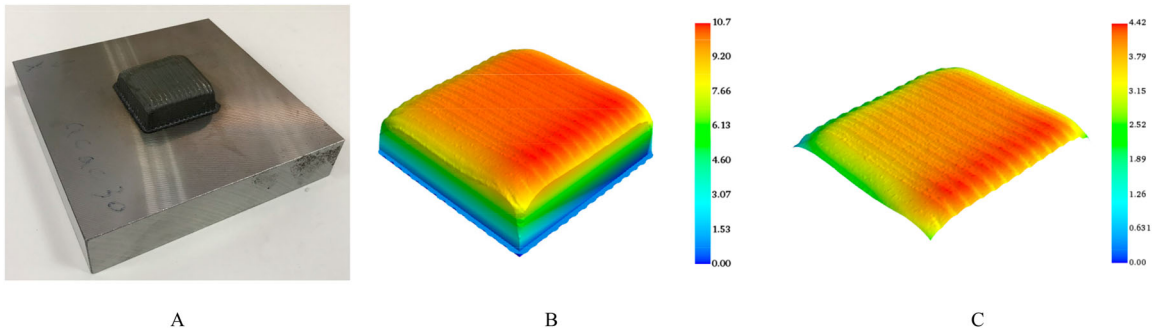

Figure 12. Top surface flatness variance calculation (unit of the colour bar is mm): (A) LAAM deposited sample; (B) 3D scanned file M; (C) trimmed scanned file $M_{trim.}$

in electronic printing (Stoyanov and Bailey 2017) and morphing shapes in 4D printing (Su et al. 2020). These methods directly applied machine learning algorithms to existing research problems in various additive manufacturing technologies. However, further machine learning model development in LAAM is limited by the constraints experienced in dataset construction. Performing metal-based additive manufacturing experiments is relatively expensive and time-consuming, inhibiting the generation of a large training dataset. The raw experimental data also contains measurement noise, increasing the workload for data pre-processing. On the contrary, the FE model provides a viable solution to address the mentioned data related problem as a well-calibrated model can provide sufficient qualified data.

The integration of the machine learning model with the FE model is critical to ensure efficient feature extraction and training of the dataset. The combination of the two models can also be designed differently to enhance modelling efficiency. For instance, the new method developed in this work integrated machine learning algorithm into the existing FE model to predict and select the infill toolpath layer by layer, as illustrated in Figure 7, whereas in our previous work, the machine learning algorithm was constructed to completely replace the FE model in thermal field prediction. Both the developed machine learning approaches were able to reduce the computational cost required by existing FE analysis. Hence, the presented work provides valuable insights into the development of more advanced machine learning integration method for simulation of multi-layered 3D deposition processing.

Table 3. Top surface flatness variance V_{fla} of the deposited cube.

	Scale	
Toolpath strategy	20 mm × 20 mm	30 mm × 30 mm
XA-YB-XC-YD	**0.4143**[a]	**0.2435**[a]
XA-YC-XA-YC	0.4628	0.4612
XA-YB-XA-YB	0.4419	0.3891
Random	0.5609	0.4111

[a]Minimum value.

4.3. Domain knowledge description

Apart from the above-mentioned consideration pertaining to integration methods, the appropriate design of the machine learning model is also important to improve prediction accuracy. Although the inner working mechanism of the machine learning is still unclear (Bahri et al. 2020), incorporating relevant domain knowledge into the machine learning model had proven to be crucial for its successful application. It should be noted that the subsequent discussion is focussed on the application of the supervised learning whereby labelled training data are prepared before the training process. The main suggestions for applying domain knowledge in machine learning model are summarised as follows:

(1) Data structure design: The raw data collected from the experiments or numerical simulation need to be processed and that usually involves translating the data into the matrix form. The physical meaning of the data has to be represented either by matrix element value or through the matrix structure (i.e. size, dimension, arrangement). Especially, the feature (input) data structure requires more elaborate consideration on the matrix representation, which is compatible with the machining learning algorithm for convergence. For instance, infill toolpath is represented using the thermal field in this work, instead of the deposition sequence number used previously (Ren et al. 2020).
(2) Algorithm structure design: Defining the input variables of the objective function requires consideration of their potential combination based on their

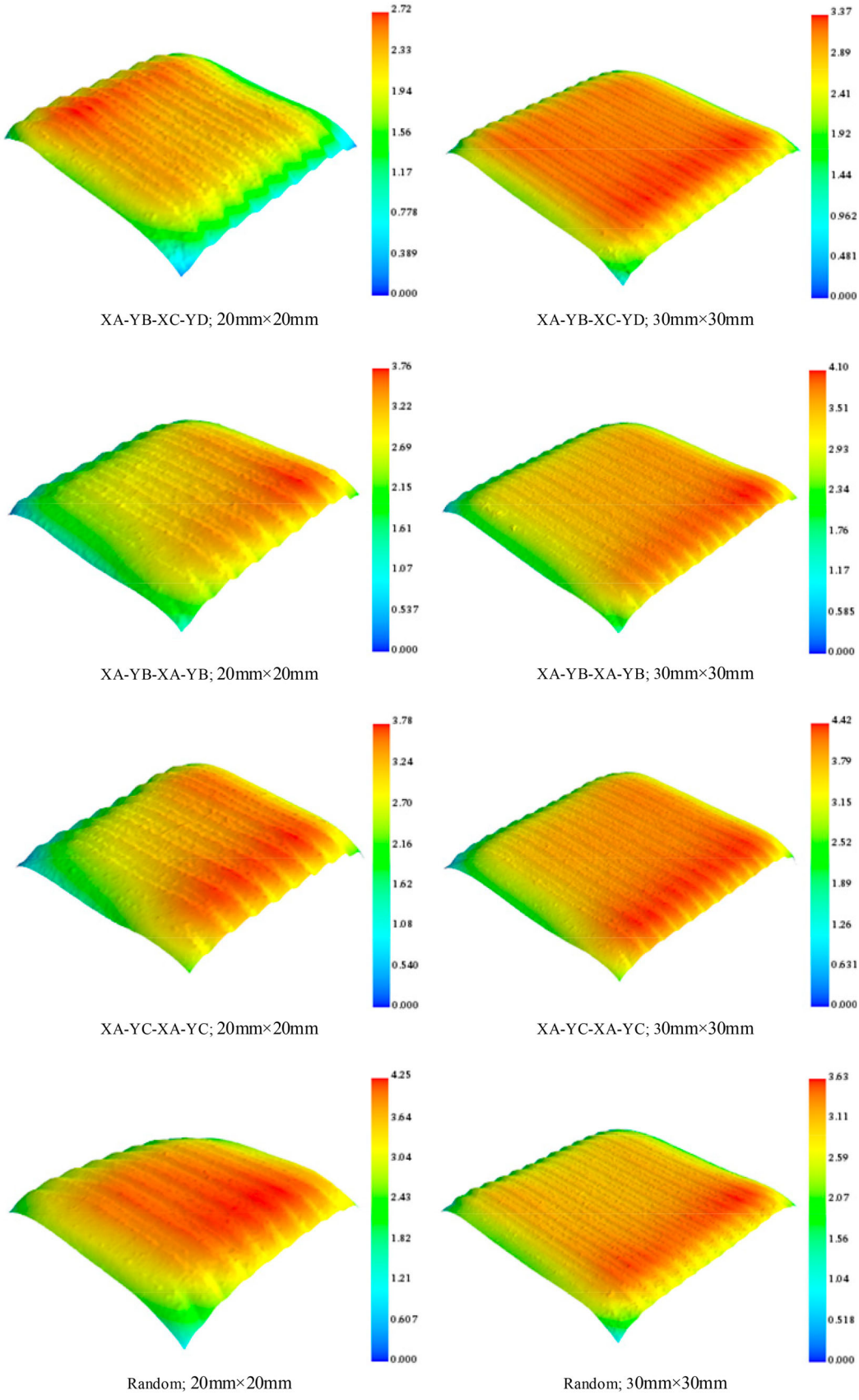

Figure 13. Trimmed scanned file M_{trim} of LAAM samples (infill toolpath strategy; scale).

physical correlation to the output parameter. This would help in selecting the appropriate neural networks to build a prototype of the machine learning model. For instance, Convolutional Neural Networks (CNN) performs well in spatial information extraction while RNN performs well in sequential information extraction.

(3) Algorithm parameter selection: Finalising the working model structure will mostly require both empirical experience and debugging. However, it was observed that increasing the complexities of the model structure did not necessarily lead to better prediction results. Compared with the number of neurons, the relation description capability of a model relies more on the algorithm structure.

5. Conclusions

The investigation on appropriate infill toolpath selection was proposed to improve the homogeneity of the temperature distribution in the LAAM process. A TP-RNN machine learning and FE model integrated infill toolpath planning approach was developed to determine the optimised infill toolpath sequence for deposition of a cube. The TP-RNN model was trained to describe the connection between the temperature fields of two previously deposited layers, selected infill toolpath and the temperature field for the next deposition layer. The integrated approach predicted that the anti-clockwise infill toolpath sequence (ABCD infill strategy) selection as the suggested optimal strategy. Experimental validation was performed and the surface flatness measurements were benchmarked against the deposition process using anti-clockwise starting position sequencing for two different cube sizes and three different deposition strategies. Future studies will focus on applying the proposed method for parts with different geometries in combination with the planning of laser process parameters such as laser power, to achieve further improvement in part quality and process consistency.

The developed approach demonstrated a novel method to integrate machine learning methods and FE models to evaluate infill toolpath in the multi-layer deposition process efficiently. The design of the data structure enables the infill toolpath planning approach to be applied in multi-layer cube deposition with different dimensions and number of layers. The developed approach structure will also be useful to enhance the predictive capability of other FE models, with consideration of more process parameters such as laser power, laser scanning speed and infill toolpaths, for toolpath planning and optimisation of multi-layer LAAM deposition process.

Acknowledgement

This research was supported by Agency for Science, Technology and Research (A*STAR), Republic of Singapore, under the IAF-PP program "Integrated large format hybrid manufacturing using wire-fed and powder-blown technology for LAAM process", Grant No: A1893a0031.

Disclosure statement

No potential conflict of interest was reported by the authors.

Funding

This research was supported by Agency for Science, Technology and Research (A*Star), Republic of Singapore, under the IAF-PP program 'Integrated large format hybrid manufacturing using wire-fed and powder-blown technology for LAAM process', Grant No: A1893a0031.

Notes on contributors

Kai Ren is a research scientist at Singapore Institute of Manufacturing Technology.

Youxiang Chew is a research scientist at Singapore Institute of Manufacturing Technology.

Ning Liu is a development scientist at Advanced Remanufacturing and Technology Centre.

Yunfeng Zhang is an associate professor at National University of Singapore.

Jerry Ying Hsi Fuh is a professor at National University of Singapore.

Guijun Bi is a senior research scientist at Singapore Institute of Manufacturing Technology.

ORCID

K. Ren http://orcid.org/0000-0002-9312-9705
N. Liu http://orcid.org/0000-0002-8517-0652
J. Y. H. Fuh http://orcid.org/0000-0002-5225-7460

References

An, Jia, Chee Kai Chua, and Vladimir Mironov. 2021. "Application of Machine Learning in 3D Bioprinting: Focus on Development of Big Data and Digital Twin." *International Journal of Bioprinting* 7 (1): 1–6.

Angelastro, A., S. L. Campanelli, and G. Casalino. 2017. "Statistical Analysis and Optimization of Direct Metal Laser Deposition of 227-F Colmonoy Nickel Alloy." *Optics & Laser Technology* 94: 138–145.

Bahri, Yasaman, Jonathan Kadmon, Jeffrey Pennington, Sam S Schoenholz, Jascha Sohl-Dickstein, and Surya Ganguli. 2020.

"Statistical Mechanics of Deep Learning." *Annual Review of Condensed Matter Physics* 11: 501–528.

Bi, Guijun, Andres Gasser, Konrad Wissenbach, Alexander Drenker, and Reinhart Poprawe. 2006. "Investigation on the Direct Laser Metallic Powder Deposition Process via Temperature Measurement." *Applied Surface Science* 253 (3): 1411–1416.

Bi, G., C. N. Sun, and A. Gasser. 2013. "Study on Influential Factors for Process Monitoring and Control in Laser Aided Additive Manufacturing." *Journal of Materials Processing Technology* 213 (3): 463–468.

Caiazzo, Fabrizia, and Alessandra Caggiano. 2018. "Laser Direct Metal Deposition of 2024 Al Alloy: Trace Geometry Prediction via Machine Learning." *Materials* 11 (3): 444.

Campanelli, Sabina Luisa, Andrea Angelastro, Carmine Gabriele Signorile, and Giuseppe Casalino. 2017. "Investigation on Direct Laser Powder Deposition of 18 Ni (300) Marage Steel Using Mathematical Model and Experimental Characterisation." *The International Journal of Advanced Manufacturing Technology* 89 (1–4): 885–895.

Chen, Lequn, Xiling Yao, Peng Xu, Seung Ki Moon, and Guijun Bi. 2020. "Rapid Surface Defect Identification for Additive Manufacturing with In-Situ Point Cloud Processing and Machine Learning." *Virtual and Physical Prototyping*, 16 (1): 50–67.

Dai, K., and L. Shaw. 2002. "Distortion Minimization of Laser-Processed Components Through Control of Laser Scanning Patterns." *Rapid Prototyping Journal* 8: 270–276.

DebRoy, T., H. L. Wei, J. S. Zuback, T. Mukherjee, J. W. Elmer, J. O. Milewski, A. M. Beese, A. Wilson-Heid, A. De, and W. Zhang. 2017. "Additive Manufacturing of Metallic Components–Process, Structure and Properties." *Progress in Materials Science* 92: 112–224.

Denlinger, Erik R, Jarred C Heigel, Pan Michaleris, and T. A. Palmer. 2015. "Effect of Inter-Layer Dwell Time on Distortion and Residual Stress in Additive Manufacturing of Titanium and Nickel Alloys." *Journal of Materials Processing Technology* 215: 123–131.

Ding, Donghong, Zengxi Pan, Dominic Cuiuri, Huijun Li, and Nathan Larkin. 2016. "Adaptive Path Planning for Wire-Feed Additive Manufacturing Using Medial Axis Transformation." *Journal of Cleaner Production* 133: 942–952.

Ding, Donghong, Zengxi Pan, Dominic Cuiuri, Huijun Li, Nathan Larkin, and Stephen Van Duin. 2016. "Automatic Multi-Direction Slicing Algorithms for Wire Based Additive Manufacturing." *Robotics and Computer-Integrated Manufacturing* 37: 139–150.

Fesharaki, Mohammad Naghiyan, Reza Shoja-Razavi, Hojjat Allah Mansouri, and Hossein Jamali. 2018. "Microstructure Investigation of Inconel 625 Coating Obtained by Laser Cladding and TIG Cladding Methods." *Surface and Coatings Technology* 353: 25–31.

Foroozmehr, Ehsan, and Radovan Kovacevic. 2010. "Effect of Path Planning on the Laser Powder Deposition Process: Thermal and Structural Evaluation." *The International Journal of Advanced Manufacturing Technology* 51 (5-8): 659–669.

Gu, D. D., W. Meiners, K. Wissenbach, and R. Poprawe. 2012. "Laser Additive Manufacturing of Metallic Components: Materials, Processes and Mechanisms." *International Materials Reviews* 57 (3): 133–164.

Haley, James C, Baolong Zheng, Umberto Scipioni Bertoli, Alexander D Dupuy, Julie M Schoenung, and Enrique J Lavernia. 2019. "Working Distance Passive Stability in Laser Directed Energy Deposition Additive Manufacturing." *Materials & Design* 161: 86–94.

Herzog, Dirk, Vanessa Seyda, Eric Wycisk, and Claus Emmelmann. 2016. "Additive Manufacturing of Metals." *Acta Materialia* 117: 371–392.

Lao, Wenxin, Mingyang Li, Teck Neng Wong, Ming Jen Tan, and Tegoeh Tjahjowidodo. 2020. "Improving Surface Finish Quality in Extrusion-Based 3D Concrete Printing Using Machine Learning-Based Extrudate Geometry Control." *Virtual and Physical Prototyping* 15 (2): 178–193.

LeCun, Yann, Yoshua Bengio, and Geoffrey Hinton. 2015. "Deep Learning." *Nature* 521 (7553): 436–444.

Lindgren, Lars-Erik, Andreas Lundbäck, Martin Fisk, Robert Pederson, and Joel Andersson. 2016. "Simulation of Additive Manufacturing Using Coupled Constitutive and Microstructure Models." *Additive Manufacturing* 12: 144–158.

Mazumder, J. 2016. "Laser-aided Direct Metal Deposition of Metals and Alloys." *Laser Additive Manufacturing: Materials, Design, Technologies, and Applications* 21–53.

Michaleris, Panagiotis. 2014. "Modeling Metal Deposition in Heat Transfer Analyses of Additive Manufacturing Processes." *Finite Elements in Analysis and Design* 86: 51–60.

Ng, Wei Long, Alvin Chan, Yew Soon Ong, and Chee Kai Chua. 2020. "Deep Learning for Fabrication and Maturation of 3D Bioprinted Tissues and Organs." *Virtual and Physical Prototyping* 15 (3): 340–358.

Nie, Zhenguo, Gang Wang, James D McGuffin-Cawley, Badri Narayanan, Shenjia Zhang, David Schwam, Michael Kottman, and Yiming Kevin Rong. 2016. "Experimental Study and Modeling of H13 Steel Deposition Using Laser Hot-Wire Additive Manufacturing." *Journal of Materials Processing Technology* 235: 171–186.

Qi, Xinbo, Guofeng Chen, Yong Li, Xuan Cheng, and Changpeng Li. 2019. "Applying Neural-Network-Based Machine Learning to Additive Manufacturing: Current Applications, Challenges, and Future Perspectives." *Engineering* 5 (4): 721–729.

Ren, K., Y. Chew, J. Y. H. Fuh, Y. F. Zhang, and G. J. Bi. 2019. "Thermo-mechanical Analyses for Optimized Path Planning in Laser Aided Additive Manufacturing Processes." *Materials & Design* 162: 80–93.

Ren, K., Y. Chew, Y. F. Zhang, G. J. Bi, and J. Y. H. Fuh. 2019. "Thermal Analyses for Optimal Scanning Pattern Evaluation in Laser Aided Additive Manufacturing." *Journal of Materials Processing Technology* 271: 178–188.

Ren, K., Y. Chew, Y. F. Zhang, J. Y. H. Fuh, and G. J. Bi. 2020. "Thermal Field Prediction for Laser Scanning Paths in Laser Aided Additive Manufacturing by Physics-Based Machine Learning." *Computer Methods in Applied Mechanics and Engineering* 362: 112734.

Ren, Lan, Todd Sparks, Jianzhong Ruan, and Frank Liou. 2010. "Integrated Process Planning for a Multiaxis Hybrid Manufacturing System." *Journal of Manufacturing Science and Engineering* 132 (2): 021006.

Ruder, Sebastian. 2016. "An Overview of Gradient Descent Optimization Algorithms." https://ruder.io/optimizing-gradient-descent/.

Song, Jie, Youxiang Chew, Guijun Bi, Xiling Yao, Baicheng Zhang, Jiaming Bai, and Seung Ki Moon. 2018. "Numerical

and Experimental Study of Laser Aided Additive Manufacturing for Melt-Pool Profile and Grain Orientation Analysis." *Materials & Design* 137: 286–297.

Stoyanov, Stoyan, and Chris Bailey. 2017. Machine Learning for Additive Manufacturing of Electronics. *Paper Presented at the 2017 40th International Spring Seminar on Electronics Technology (ISSE)*.

Su, Jheng-Wun, Dawei Li, Yunchao Xie, Thomas Zhou, Wenxin Gao, Heng Deng, Ming Xin, and Jian Lin. 2020. "A Machine Learning Workflow for 4D Printing: Understand and Predict Morphing Behaviors of Printed Active Structures." *Smart Materials and Structures* 30 (1): 015028.

Tan, Joel Heang Kuan, Swee Leong Sing, and Wai Yee Yeong. 2020. "Microstructure Modelling for Metallic Additive Manufacturing: A Review." *Virtual and Physical Prototyping* 15 (1): 87–105.

Venturini, Giuseppe, Filippo Montevecchi, Francesco Bandini, Antonio Scippa, and Gianni Campatelli. 2018. "Feature based Three Axes Computer Aided Manufacturing Software for Wire arc Additive Manufacturing Dedicated to Thin Walled Components." *Additive Manufacturing* 22: 643–657.

Yan, Hui, Lida Shen, Xiao Wang, Zongjun Tian, Guojian Xu, Deqiao Xie, and Huixin Liang. 2018. "Stress and Deformation Evaluation of the Subarea Scanning Effect in Direct Laser-Deposited Ti-6Al-4V." *The International Journal of Advanced Manufacturing Technology* 97 (1-4): 915–926.

Yu, Jun, Xin Lin, Liang Ma, Junjie Wang, Xingling Fu, Jing Chen, and Weidong Huang. 2011. "Influence of Laser Deposition Patterns on Part Distortion, Interior Quality and Mechanical Properties by Laser Solid Forming (LSF)." *Materials Science and Engineering: A* 528 (3): 1094–1104.

Zhang, Yingjie, Geok Soon Hong, Dongsen Ye, Kunpeng Zhu, and Jerry YH Fuh. 2018. "Extraction and Evaluation of Melt Pool, Plume and Spatter Information for Powder-bed Fusion AM Process Monitoring." *Materials & Design* 156: 458–469.

Zhang, Xinchang, Wei Li, Xueyang Chen, Wenyuan Cui, and Frank Liou. 2018. "Evaluation of Component Repair Using Direct Metal Deposition from Scanned Data." *The International Journal of Advanced Manufacturing Technology* 95 (9–12): 3335–3348.